# A New Positioning Algorithm for Position-Sensitive Avalanche Photodiodes

Jin Zhang, *Member, IEEE*, Peter D. Olcott, *Member, IEEE*, and Craig S. Levin, *Member, IEEE*

***Abstract*—We are using a novel position sensitive avalanche photodiode (PSAPD) for the construction of a high resolution positron emission tomography (PET) camera. Up to now most researchers working with PSAPDs have been using an Anger-like positioning algorithm involving the four corner readout signals of the PSAPD. This algorithm yields a significant non-linear spatial "pin-cushion" distortion in raw crystal positioning histograms. In this paper, we report an improved positioning algorithm, which combines two diagonal corner signals of the PSAPD followed by a 45° rotation to determine the X or Y position of the interaction. We present flood positioning histogram data generated with the old and new positioning algorithms using a $3 \times 4$ array of $2 \times 2 \times 3$ mm$^3$ and a $3 \times 8$ array of $1 \times 1 \times 3$ mm$^3$ of LSO crystals coupled to $8 \times 8$ mm$^2$ PSAPDs. This new algorithm significantly reduces the pin-cushion distortion in raw flood histogram image.**

***Index Terms*—Avalanche photodiode, positioning algorithm, positron emission tomography.**

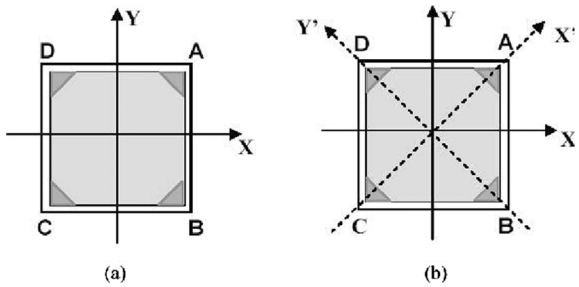


Fig. 1. Position sensitive square PSAPD detector with corner contacts labeled A, B, C, D. The signals generated on these contacts are used to accurately position light flashes that hit the photodetector. (a) X and Y coordinates determined by Anger logic algorithm [see (1)]; (b) the new diagonal algorithm determines X' and Y' using diagonal channels and then the image is rotated by $\pi/4$ to have same orientation as the Anger logic algorithm [see (2) and (3)].

## I. Introduction

MEDICAL radionuclide imaging cameras (SPECT or PET) comprise a position sensitive array of scintillation crystals coupled to photodetectors such as photomultiplier tubes (PMTs) or photodiodes. An incoming high energy photon is absorbed in the crystal, which results in a flash of light that is positioned using the distribution of electronic signals produced in the photodetector array. In scintillation detectors that use position sensitive avalanche photodiodes (PSAPDs), an algorithm similar to Anger logic [1] is typically used to position events using the resulting four corner anode signals [2]–[5]. However, because of the positioning non-linearity inherent in a detector comprising a resistive sheet with corner contacts [4], the flood histogram generated using Anger's positioning algorithm for the PSAPD shows a well-known "pin-cushion" distorted shape [1]–[5]. The standard algorithm can be expressed as:

$$X = \frac{(A+B)-(C+D)}{A+B+C+D}$$
$$Y = \frac{(A+D)-(B+C)}{A+B+C+D} \quad (1)$$

where A, B, C and D are the digitized pulse heights collected from the four corner anodes in the detector and X, Y are the coordinates determined for each annihilation photon interaction. Fig. 1(a) schematically illustrates a square-shaped PSAPD with four readout corners and X-Y coordinates determined by (1).

The standard PSAPD is packaged on a ceramic substrate [4]. For our particular PET detector design [see Fig. 2(a)] [2], [6] novel thin PSAPDs have been developed by Radiation Monitoring Devices, Inc (Watertown, MA). This type of PSAPD uses a 200-$\mu$m thick silicon chip packaged on a 50-$\mu$m thick polyimide (Kapton) "flex" circuit [Fig. 2(a)]. The proposed detector design uses an "edge-on" orientation, with incoming normal incidence photons entering parallel to the PSAPD chip. This design has $\sim$1 mm resolution with directly measured photon interaction depth in $\sim$2 cm effective LSO thickness and $>$90% scintillation light collection efficiency [2], [6] [see Fig. 2(b)]. We have studied performance of both the standard ceramic-mounted PSAPD and thin flex-mounted PSAPD [7], [8]. In both detectors, the flood histograms generated by the Anger-type positioning algorithm (1) show significant pin-cushion distortion. This distortion makes it difficult to perform the process of crystal segmentation from the flood histogram that is required to study and calibrate parameters such as crystal location, spatial resolution, energy resolution, and coincidence time resolution for individual crystals. In this paper, we report a new positioning algorithm for PSAPDs which generates images with significantly less "pin-cushion" distortion.

## II. Materials and Methods

The new algorithm combines only the signals from the diagonal channels to determine an X' and Y' position in a rotated coordinate system within the image plane and then rotates the

Manuscript received January 31, 2006; revised December 28, 2006. This work was supported in part by NIH-NCI under Grants R01 CA119056 and R21 CA098691, and by NIBIB under Grant R21/R33 EB003283.

J. Zhang was with the Department of Radiology and Molecular Imaging Program, Stanford University, Stanford, CA 94305 USA. He is now with PerkinElmer Optoelectronics, Santa Clara, CA 95054 USA (e-mail: zhangjin2004@gmail.com).

P. D. Olcott and C. S. Levin are with the Department of Radiology and Molecular Imaging Program, Stanford University, Stanford, CA 94305 USA (e-mail: pdo@stanford.edu; cslevin@stanford.edu).

Color versions of one or more of the figures in this paper are available online at http://ieeexplore.ieee.org.

Digital Object Identifier 10.1109/TNS.2007.894129

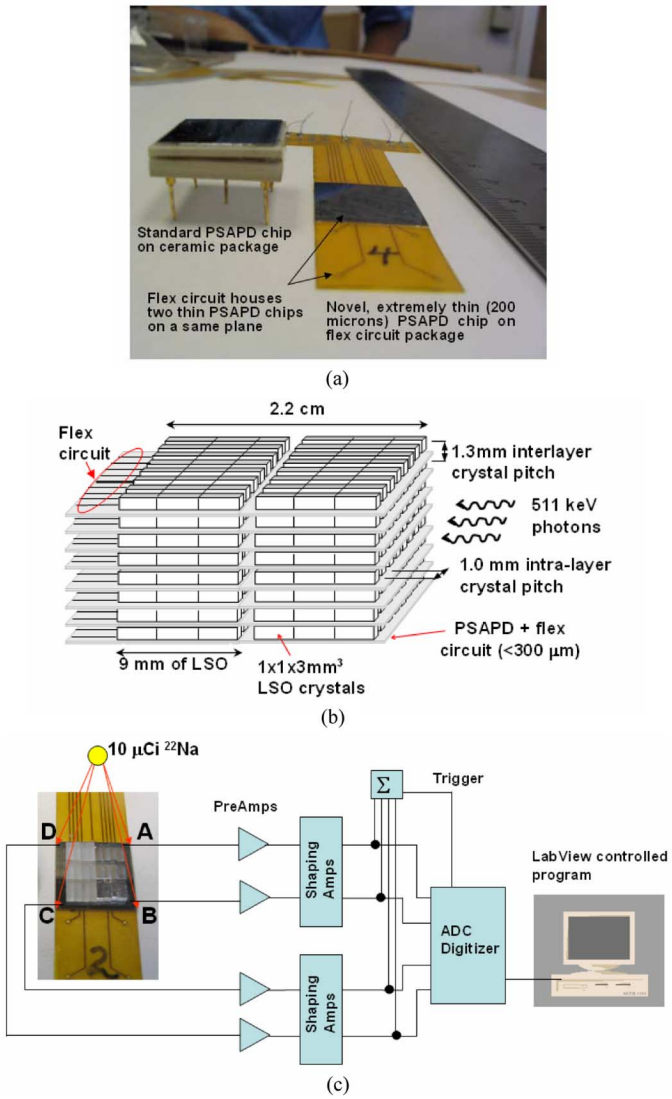


Fig. 2. (a) Picture of the standard (left) and new thin PSAPD (right) developed for high resolution PET; (b) Schematic of a block detector module for the development of a dedicated PET camera with "edge-on" geometrical configuration. (c) Schematic of experimental setup used to digitize the four corner signals of the PSAPD.

image by 45° to determine the correct orientation. The new algorithm can be simply expressed as:

$$X' = \frac{A - C}{A + C}$$
$$Y' = -\frac{B - D}{B + D}, \quad (2)$$
$$X = X' \cos\left(\frac{\pi}{4}\right) + Y' \sin\left(\frac{\pi}{4}\right)$$
$$Y = Y' \cos\left(\frac{\pi}{4}\right) - X' \sin\left(\frac{\pi}{4}\right), \quad (3)$$

where A, B C and D are again the digitized signals from the four channels as shown in Fig. 1(b).

Experimental data were acquired with both standard and thin PSAPDs with a 10 $\mu$Ci Na-22 point source flood irradiation. Both a $3 \times 4$ array of $2 \times 2 \times 3$ mm$^3$ and $3 \times 8$ array of $1 \times 1 \times 3$ mm$^3$ LSO crystals were coupled to the PSAPDs. For

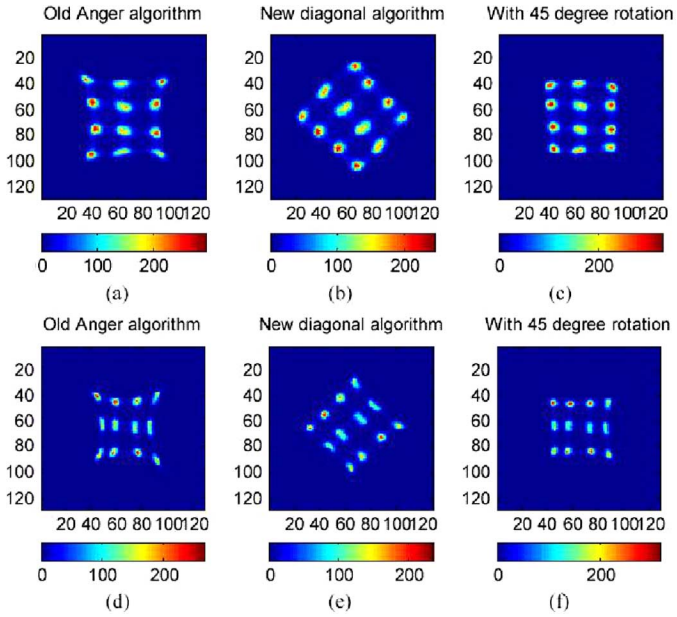


Fig. 3. Flood images generated by the Anger-like algorithm [(a) and (d)] and the new algorithm [(b) and (e) before rotation, (c) and (f) after rotation] using a $3 \times 4$ array of $2 \times 2 \times 3$ mm$^3$ LSO crystals coupled to a PSAPD. The flood images (a) to (c) were acquired with the standard PSAPD and images (d) to (f) with the new thin PSAPD.

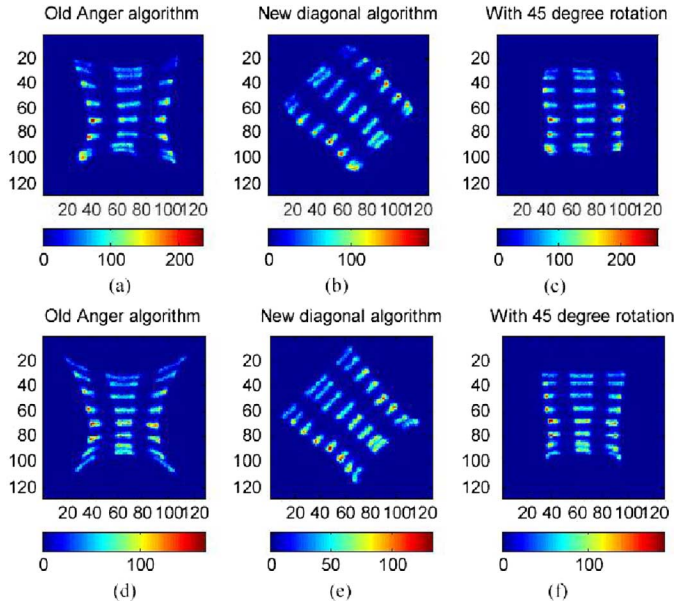


Fig. 4. Flood images generated by the Anger-like algorithm [(a) and (d)] and the new algorithm [(b) and (e) before rotation, (c) and (f) after rotation] using a $3 \times 8$ array of $1 \times 1 \times 3$ mm$^3$ LSO crystals coupled to a PSAPD. The flood images (a) to (c) were acquired with the standard PSAPD and the images (d) to (f) with the new thin PSAPD.

the $3 \times 8$ array of crystals, to study the effect of crystal surface finish on event positioning, half of the array (12 crystals) had a polished surface treatment while the other half (12 crystals) had ground surfaces. The $3 \times 4$ array of $2 \times 2 \times 3$ mm$^3$ LSO crystals had all ground ("as cut") surface finish. The experimental setup is shown in Fig. 2(c). Signals from the four corner anode contacts of the PSAPD were input into a charge-sensitive pre-amplifier (Cremat 110) and then further amplified

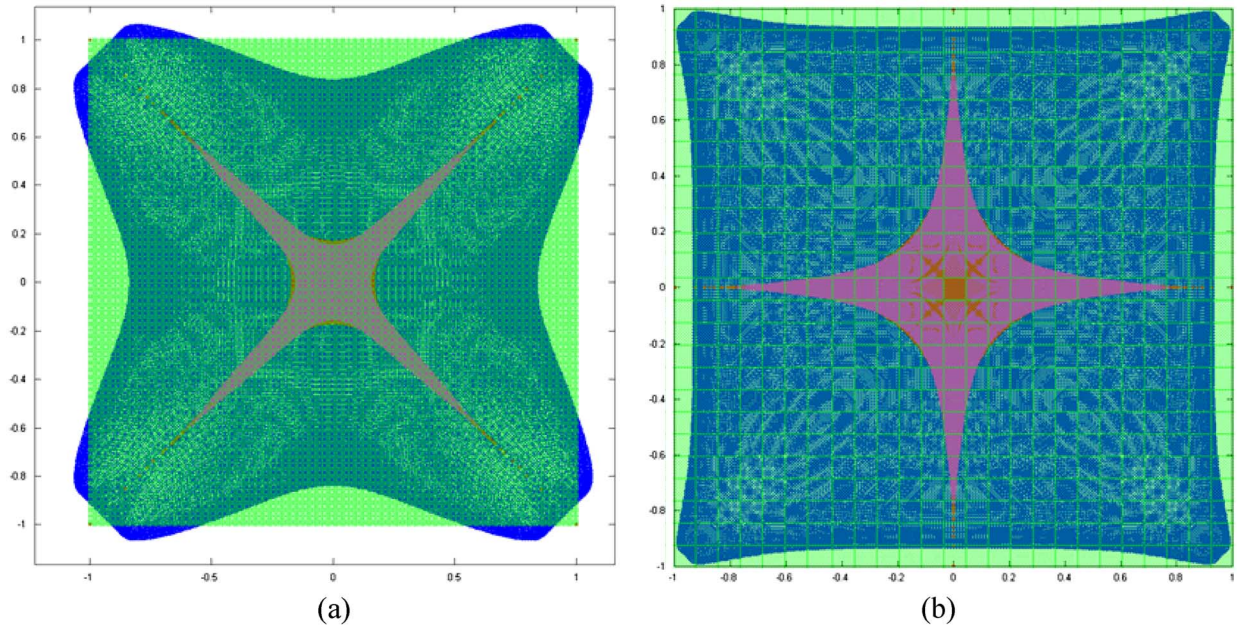


Fig. 5. Finite element model simulation results: (a) The polynomial functions generated by Anger-type algorithm (dark red surface) and the ideal sheet (green square mesh) are mis-matched. The dark blue surface is the inversion of the polynomial (red) applied to the FEM simulation. A perfect inversion would produce a perfectly square grid (green mesh). The polynomial has problem inverting at the singularities (dark blue mesh with pincushion distortion at the four edges and blow-out at the corners). (b) With the new diagonal algorithm, the match between the green and dark blue meshes is significantly improved. The inversion of the polynomial fitting (dark blue mesh) covers most of the green surface.

by shaping amplifiers (EG&G Ortec 855 Dual Channel Spec Amplifiers) with a 500 ns shaping time. Each of the four output signals was split into two branches, one branch of the output from each channel was summed to generate a digitization trigger signal; the four analog signals in the other branch were digitized by a Labview program controlled four-channel analog-to-digital converter (ADC) (National Instruments). The data were stored in list mode for post-processing. Individual crystal energy spectra, FWHM energy resolution, and photon counts in a FWHM energy window centered at the 511 keV photopeak were extracted by segmentation of the crystals from the flood histogram image.

To understand the difference between the two algorithms in positioning events, the sheet resistance distribution at the surface of the detector was studied with a finite element model (FEM) simulation [9]. As it is complicated to find an analytical solution to the problem of calculating the charge splitting on a square chip, we used a FEM method to simulate a resistive sheet with four read-out conductors at the corners by solving the Laplace's equation for this sheet. The basic idea is, assuming a uniform resistive sheet with four contacts, the amount of charge split to a corner contact is proportional to the reciprocal of the distance between the injection point of charge (where scintillation photons are converted to electrons) and this corner contact (where the electrons are collected) [9]. With a linear center of mass positioning algorithm, the resistive sheet has a non-linear mapping between event location and the detected position. With the assumption that the entire process from 511 keV photon interaction in the scintillator through event positioning may be described as a one-to-one mapping, one can invert the operator that maps the event position to detected position to correct the position non-linearity. This operator, a polynomial function, was derived from the FEM simulation (with a $201 \times 201$ mesh grid) by solving the Laplace's equation on a resistive sheet with four corner contacts [9]. The details of this FEM simulation were introduced in [9] and will not be reviewed in this paper.

## III. Results

Fig. 3 shows flood histograms generated using both the Anger-type algorithm and our new algorithm for the standard and thin PSAPDs with the $4 \times 3$ array of $2 \times 2 \times 3$ mm$^3$ LSO crystals. Fig. 3(a) shows results using the Anger-type positioning algorithm, Fig. 3(b) shows the flood histogram formed with X' and Y' calculated using (2), and Fig. 3(c) is the rotated image with X and Y calculated using (3). We observe that crystal flood images generated by the Anger-like algorithm [Fig. 3(a) and (d)] have strong pin-cushion distortion. The positioning histogram image measured with the new thin PSAPD [Fig. 3(d)] is more distorted than the standard PSAPD image [Fig. 3(a)] mainly due to a slightly lower sheet resistance of this device.

Flood images acquired with both PSAPD detectors coupled to the $3 \times 8$ array of $1 \times 1 \times 3$ mm$^3$ LSO crystals are shown in Fig. 4. The pin-cushion distortion in both images generated by the Anger-type algorithm is strong [Fig. 4(a)], and again worse for the new thin PSAPD [Fig. 4(d)]. On the other hand, images generated by the new algorithm are almost free of pin-cushion distortion [Fig. 4(c) and (f)] regardless of devices. Recall that the upper $3 \times 4$ crystals in the flood images have ground surfaces and the lower $3 \times 4$ crystals have polished surfaces. Consequently, in each image, the upper $3 \times 4$ crystals are slightly larger than the lower $3 \times 4$ crystals in size. It is also noticed that the new algorithm generated a slight "barrel" distortion for the

standard PSAPD [Fig. 4(c)], which is fabricated on a ceramic substrate.

Through a FEM simulation study on the charge distribution within a square resistive sheet, we notice that, with the Anger-like algorithm, the polynomial function shows evident pin-cushion on all edges [pink mesh, Fig. 5(a)]. The inversion of this polynomial function [blue mesh, Fig. 5(a)] still shows evident pin-cushion distortions. A perfect inversion would produce a perfectly square grid (green square). The inverted polynomial fitting clearly has mismatch at the singularities along the edges and at the corners. With our new algorithm, however, the inversion of the polynomial correction function has shown much better uniformity at the edges on the $201 \times 201$ mesh grid, as shown in the blue layer in Fig. 5(b). We noticed that the polynomial fitting for our new algorithm covers a significantly larger area than that of the Anger-like algorithm. This illustrates that the new diagonal positioning algorithm, with much less pin-cushion distortion, facilitates a more linear mapping to the true event position on the planar resistive sheet than the Anger-type version.

Fig. 6 shows the crystal boundaries drawn on the flood histogram during the crystal segmentation process for events positioned with the Anger-like and new algorithms. Fig. 7 shows the individual crystal counts, photopeak pulse heights, and energy resolution values generated from the crystal segmentation process using the Anger-type and new positioning algorithms.

## IV. Discussion

The pin-cushion distortion is a serious problem when crystal segmentation is required to measure and calibrate energy resolution and crystal location for tiny individual crystals from a flood positioning histogram. In a calibration step for a PET system, individual crystals are mapped with a look-up table to determine parameters such as energy and coincidence time windows and efficiencies for individual crystals. With an Anger-like algorithm, an automatic algorithm for crystal segmentation from the flood image is not possible for crystals near the corner of the PSAPD because of the severe pin-cushion distortion. The new positioning algorithm presented in this work allows one to use a relatively simple segmentation algorithm from the raw (unprocessed) flood data set. This substantially simplifies the creation of positioning look-up calibration tables that have to be generated for every LSO-PSAPD positioning detector present in the proposed PET system.

As shown in Fig. 6(a), we noticed that the crystal segmentation process bisected corner crystals and the calculated crystal boundaries were not correct. Thus, a semi-empirical method must be used for segmentation of these crystals. Polynomial fitting can be used to correct the pin-cushion distortion but cannot perfectly recover linearity [9]. Shah *et al.* studied the flood histogram with a standard PSAPD and they used a previously generated response map to correct this pin-cushion distortion [4]. However, with the new diagonal algorithm, the raw image is already adequate for automatic crystal segmentation and no precorrections to the image are needed, as shown in Fig. 6(b). This simplifies the segmentation of the flood image and therefore helps on the determination of crystal position, energy window and time window settings, and also efficiency look-up tables for individual crystals.

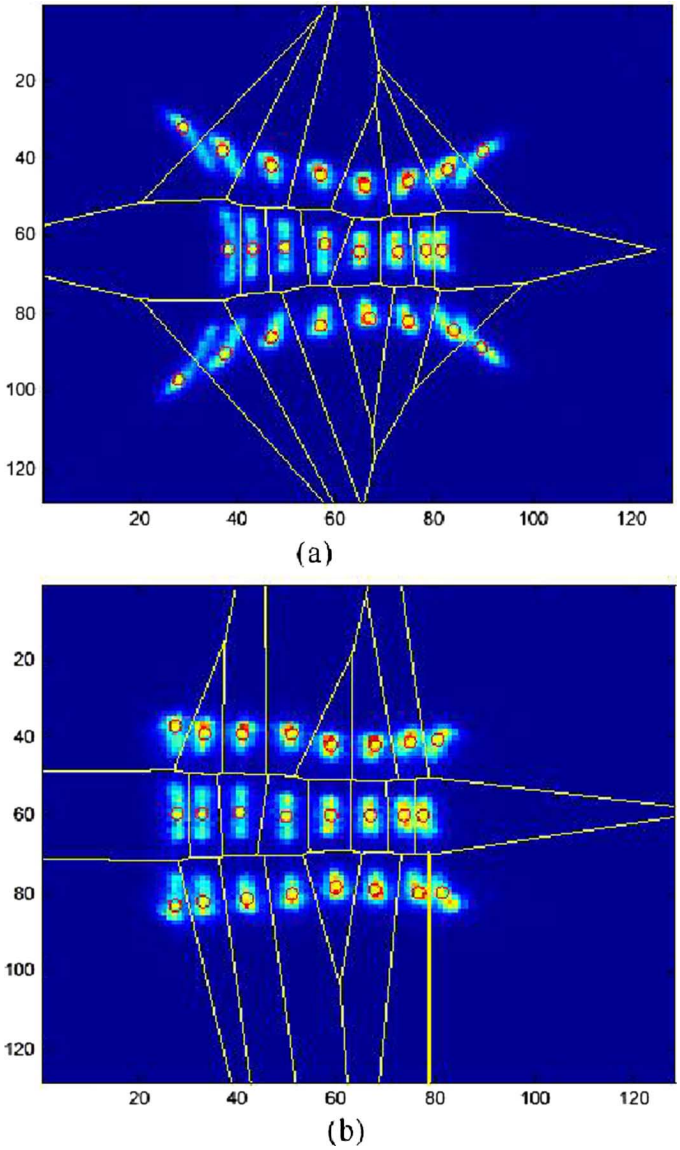


Fig. 6. Calculated crystal segmentation lines superimposed on top of the of the crystal flood histogram acquired using the new thin PSAPD with a $3 \times 8$ array of $1 \times 1 \times 3$ mm$^3$ LSO crystals (a) using an Anger-like algorithm, (b) with the new algorithm. The left $3 \times 4$ crystals had ground surfaces and the right $3 \times 4$ crystals had polished surfaces.

Fig. 7 shows energy resolution and efficiency results generated from segmentation of individual crystals with both algorithms for the thin PSAPD. We observed that the new algorithm gave a more uniform result for photon counts [Fig. 7(d)] in individual crystals compared to that observed with the Anger-like algorithm [Fig. 7(a)]. As for photopeak position and energy resolution, both algorithms gave comparable results [Fig. 7(b)–(c) and (e)–(f)]. More detailed study of the energy, coincidence time and spatial resolution of the PSAPD has been accomplished and will be reported separately [8], and therefore, is not discussed in details in this paper.

The physical reason that our new algorithm generates much less pin-cushion distortion has been studied [9]. It is believed that this is mainly due to the more linear charge sharing along

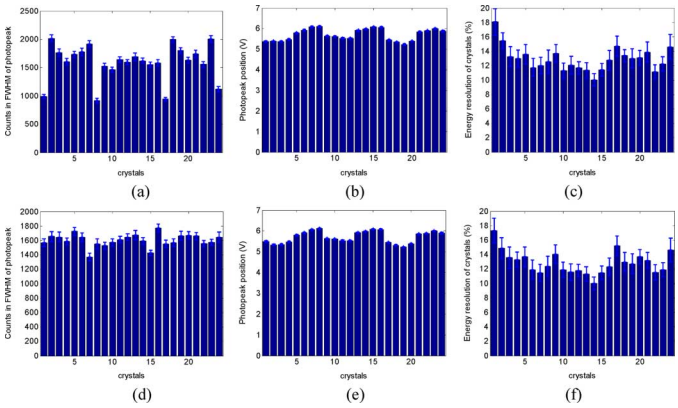


Fig. 7. Analysis of individual crystal performance for a $3 \times 8$ array of $1 \times 1 \times 3$ mm$^3$ LSO crystals coupled to new thin PSAPD using the Anger-like algorithm ((a) to (c)) and the new algorithm [(d) to (f)]. Plotted are crystal efficiencies within the FWHM of the photopeak [(a) and (d)], photopeak position in the energy spectrum [(b) and (e)], FWHM of photopeak energy resolution [(c) and (f)] for each of the 24 individual crystals.

the diagonal directions of the resistive sheet compared to that along the directions parallel to the resistive sheet edges. The positioning dynamic range in raw flood histogram image is significantly improved using the new algorithm. The measured data and FEM simulation study clearly illustrate the advantage of the new algorithm over the traditional Anger-type positioning algorithm.

## V. Conclusion

A new scintillation event positioning algorithm for PSAPDs has been described. This algorithm uses diagonally opposing readout channels to determine the centroid of a scintillation flash. Measurements with the new thin PSAPD we have developed for high resolution PET have clearly demonstrated that, with this new event positioning algorithm, raw flood histogram images are almost distortion free as compared to the images generated by the traditional Anger-type algorithm. Using the new positioning algorithm, no linearity corrections were needed and successful and accurate crystal segmentation could be applied to raw flood histogram data. This helps to simplify the determination of individual crystal position, energy and efficiency performance and also the associated efficiency look-up tables.

## Acknowledgment

The authors would like to thank colleagues A. Foudray, Dr. G. Chinn, and Dr. F. Habte for useful discussions and help in experiments.

## References

[1] H. O. Anger, "Scintillation camera with multichannel collimators," *J. Nucl. Med.*, vol. 65, pp. 515–531, 1964.

[2] C. S. Levin, A. M. K. Foudray, P. D. Olcott, and F. Habte, "Investigation of position sensitive avalanche photodiodes for a new high-resolution PET detector design," *IEEE Trans. Nucl. Sci.*, vol. 51, no. 3, pp. 805–810, Jun. 2004.

[3] K. C. Burr, A. Ivan, D. E. Castleberry, J. W. LeBlanc, K. S. Shah, and R. Farrell, "Evaluation of a prototype small-animal PET detector with depth-of-interaction encoding," *IEEE Trans. Nucl. Sci.*, vol. 51, no. 4, pp. 1791–1798, Aug. 2004.

[4] K. S. Shah, R. Farrell, R. Grazioso, E. S. Harmon, and E. Karplus, "Position-sensitive avalanche photodiodes for Gamma-ray imaging," *IEEE Trans. Nucl. Sci.*, vol. 49, no. 4, pp. 1687–1692, Aug. 2002.

[5] P. A. Dokhale, R. W. Silverman, K. S. Shah, R. Grazioso, R. Farell, J. Glodo, M. A. MeClish, G. Entine, V. H. Tran, and S. R. Cherry, "Performance measurements of a depth-encoding PET detector module based on position sensitive avalanche photodiode read-out," *Phys. Med. Biol.*, vol. 49, pp. 4293–4304, 2004.

[6] C. S. Levin, "Design of a high-resolution and high-sensitivity scintillation crystal array for PET with nearly complete light collection," *IEEE Trans. Nucl. Sci.*, vol. 49, no. 5, pp. 2236–2243, Oct. 2002.

[7] C. S. Levin, J. Zhang, A. M. K. Foudray, R. Farrell, P. D. Olcott, M. McClish, F. Habte, and K. S. Shah, "A thin position sensitive avalanche photodiode for ultra-high resolution PET," presented at the 2004 IEEE Nuclear Science Symp. and Medical Imaging Conf., Abstract #M5-130, Book of Abstracts, p. 164, IEEE Nuclear and Plasma Science Society.

[8] J. Zhang, A. M. K. Foudray, P. D. Olcott, and C. S. Levin, "Performance characterization of a novel thin position-sensitive avalanche photodiode for high resolution PET camera," in *Proc. IEEE Nuclear Science Symp. Conf. Rec.*, 2005, vol. 5, pp. 2478–2482.

[9] P. D. Olcott, J. Zhang, C. S. Levin, F. Habte, and A. M. K. Foudray, "Finite element model based spatial linearity correction for scintillation detectors that use position sensitive avalanche photodiodes," in *Proc. IEEE Nuclear Science Symp. Conf. Rec.*, 2005, vol. 5, pp. 2459–2462.